Real fluid effects on Shock Tube flow at supercritical conditions

Sai Praneeth[1]
Mechanical & Mechatronics Engineering, University of Waterloo, ON, Canada

(Dated: December 4, 2017)

Submitted for course project report on High speed & compressible flows ME 765

A study on shock tube simulations under supercritical thermodynamic conditions to investigate real fluid effects on the wave propagation. The numerical methods are an approximate riemann solver modified for real fluid thermodynamics. Three cases are studied supercriticial, nearcritical and subcritical conditions. Also an attempt has been made to study the transcritical case using the double flux method, but the spurious pressure oscillations failed the simulation.

I. INTRODUCTION

Shock tube problems are of great use when it comes to validating numerical codes/schemes for various characteristics like shock capturing, dissipation, preventing oscillations etc. A fluid is said to be in a supercritical state, if its thermodynamic temperature and pressure are above its critical point. Since it is difficult to use experiments to validate the supercritical flow behaviour, often times simulations are widely used. Especially in the cases of supercritical fuel injection in diesel engines, mixing and injection of cryogenic propellants in rocket engines, organic rankine cycle turbines. The present study aims at understanding the influence of supercritical, nearcritical, subcritical theromdyanmic conditions on the shock tube flow especially the shock wave, expansion fan locations in each case. It is well known that the supercritical fluids have special thermodynamic properties by having a liquid like high density and gas like high diffusivity. As we reach near the critical point, the specifc heat increases rapidly as shown in the figure 1. which causes a large expansion even for small increase in temperature. This makes perfect gas assumption invalid and needs accurate calculation of thermodynamic properties.

There have been several attempts in studying shock tube flow in supercritical and nearcritical conditions, Near the critical point the compression by shock introduces a phase transition, and non-classical waves are observed as a result of the thermodynamic property changes.[13] The application of accurate equation of states to the gas dynamics simulation revealed the formation of non-classical supersonic wave[17]. Arina[10] developed a numerical method for investigating supercritical fluid flow in nozzles, shock tube using cubic equation of states. Terashima[1],[16] presented a high resolution numerical method for simulating supercritical flows with large density variations and was able to resolve the flow interfaces over a wide range of scales. There have been several extensions of Riemann solvers to the real fluid thermodynamic conditions, specifically for van der Waals eqation of state[9],[13], stiff-gas equation of state[18], cubic equation of states[11].

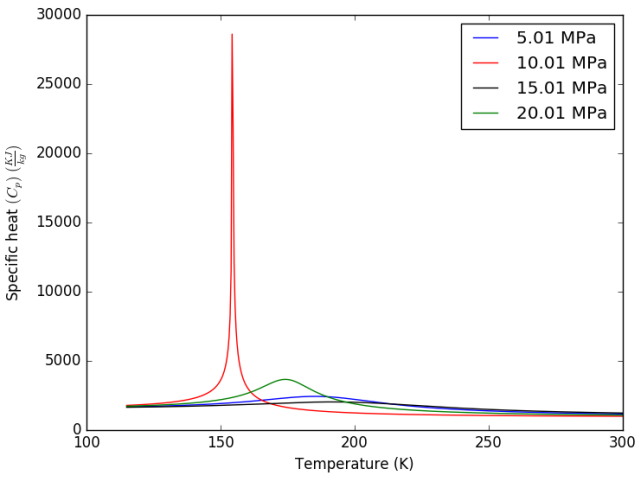

Figure 1. Specific heat (C_p) vs Temperature plot for Oxygen

The aim of the present work is to modify the existing HLLC approximate riemann solver for real fluid flows, there by using accurate thermodynamic properties for calculating wave speeds with a possibility to access various types of equation of states (cubic, tabular, perfect gas). The numerical scheme consists of a modified HLLC riemann solver for a single phase real fluid at nearcritical, supercritical conditions. The shock tube simulations are performed for three cases, the supercritical case, the nearcritical case and the subcritical case.

II. NUMERICAL METHODOLOGY

1. Governing equations

The governing equations are two dimensional euler equations, Approximate riemann solvers HLLC[3] and a solver based on Colella and Glaz[6] method are used for evaluating the inviscid fluxes across the interfaces. (Each one as an individual scheme) To obtain second-order accurate spatial and temporal discretization in both directions, the fluxes on each interface (left and right in each direction) are reconstructed in piecewise linear method

with a 4th order monotonized central difference (MC) limiter. The third order total variation diminishing TVD Runge-Kutta[2] scheme is used for time integration.

$$\frac{\partial \rho}{\partial t} + \nabla.(\rho \mathbf{u}) = 0 \tag{1}$$

$$\frac{\partial \rho \mathbf{u}}{\partial t} + \nabla.(\rho \mathbf{u}\mathbf{u} + p\mathbf{I}) = 0 \tag{2}$$

$$\frac{\partial E}{\partial t} + \nabla.(E\mathbf{u} + p.\mathbf{I}.\mathbf{u}) = 0 \tag{3}$$

Here, ρ is the density, $\mathbf{u}$ is the velocity vector, p is the static pressure, E is the total energy and I is the unit vector.

2. Equation of state

To close the compressible euler equations and to accurately evaluate the thermodynamic properties under supercritical conditions, the coolprop[4] libray is employed, in which the thermodynamic properties are calculated using a Helmholtz-energy based equation of state. Other empirical equation of states that are widely used in supercritical fluid simulations are Peng-Robinson and Soave-Redlich Kwong, both equations are easy to compute but cannot maintain accuracy in the near critical regime. In this Helmholtz-energy based approach[4], the dimensionless Helmholtz energy α is written as,

$$\alpha = \alpha^0 + \alpha^r \tag{4}$$

Where α^r is the residual part and α^0 is the ideal gas part. With this formulation, the other thermodynamic properties (pressure, temperature, density, enthalpy, etc..,) can be calculated using the derivatives of those two parts. As an example, to calculate pressure analytically as in the before mentioned method,

$$Z = \frac{p}{\rho RT} = 1 + \delta\left(\frac{\partial \alpha^r}{\partial \alpha^0}\right) \tag{5}$$

Where Z is the compressibility factor, p is the pressure and ρ is the density, R is the specific gas constat, T is the temperature and δ is the reduced density given by $\delta = \frac{\rho}{\rho_{red}}$, ρ_{red} is the reciprocal reduced pressure[4].

3. Spatial discretization and temporal integration schemes

Due to the inherent simple characteristic structure, the conserved variables are converted into the primitive variables before reconstruction. As mentioned previously, we used a piecewise linear reconstruction approach where the cell's average of variables is approximated with a line having non-zero slope. As this method is second order accurate in space and time, occurrence of oscillations at the discontinuities, contact interfaces are normal. To prevent such oscillations a MC limiter[5] (monotonized central difference) is used to limit the slopes at extrema and further and guarantee that no new maxima or minima will occur. For temporal integration, a third-order total variation diminishing TVD Runge-kutta method is used.

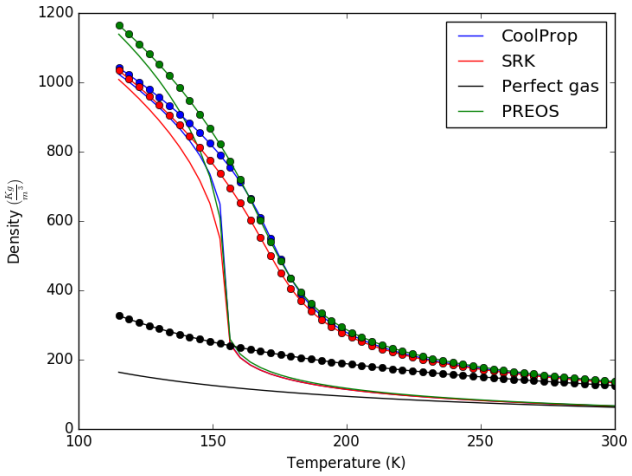

Figure 2. Density vs Temperature plot for two pressures (O - 10.01 MPa, - 5.01 MPa) for Oxygen

4. Real fluid modification for HLLC approximate Riemann solver

The original HLLC approximate riemann solvers is formulated based on a constant gamma (γ) equation of state, as we know that the thermodynamic properties vary rapidly as we approach the near critical temperature and pressure making the perfect gas assumption invalid. Also, there is a fundamental assumption[7] that the wave speed estimates that are based on speed of sound are valid for a given equation of state. Hence, the equation of state would only be needed to compute the speed of sound thereby the wave speeds (both left & right). Inorder to incorporate the real fluid effects into the HLLC solver, there are two solutions, one[18] is carrying thermodynamic index γ_e using an evolution equation and another is to carry ρe which is calculated at the interface states in addition to the primitive variables ρ, u, p. Although this approach overfits the thermodynamics, it prevents the need to calculate γ_e as described in the first method. In the current project, the Colella and Glaz method[6] is used and the effective thermodynamic index is written as,

$$\gamma_e = \frac{p}{\rho e} + 1 \tag{6}$$

And then the characteristics for the euler equations are solved where the speed of sound is calculate using the above mentioned thermodynamic index in perfect gas assumption for a given cell.

III. RESULTS AND DISCUSSIONS

1. Validation

Previously Terashima[1] carried out a simulation of shock tube under supercritical thermodynamic conditions, for this problem carbon dioxide is considered as the working fluid whose critical pressure, temperature and density[8] are $T_{crit} = 304.22K, p_{crit} = 7.37MPa, \rho_{crit} = 348.8\frac{kg}{m^3}$. The initial conditions for this sod shocktube simulation are

$$(\rho, u, p) = \begin{cases} (\rho_0, 0.0, 10p_0) & 0 \leq x \leq 0.5 \text{ m}, \\ (0.01\rho_0, 0.0, 0.1p_0) & 0.5 \leq x \leq 1.0 \text{ m} \end{cases}$$

Here, $\rho_0 = \rho_{crit} = 348.8\frac{Kg}{m^3}$, and $p_0 = p_{crit} = 7.37MPa$, the grid consists of 2001 x 4 uniformly distributed cells. The below plot is taken at t = 2.745E-04 s.

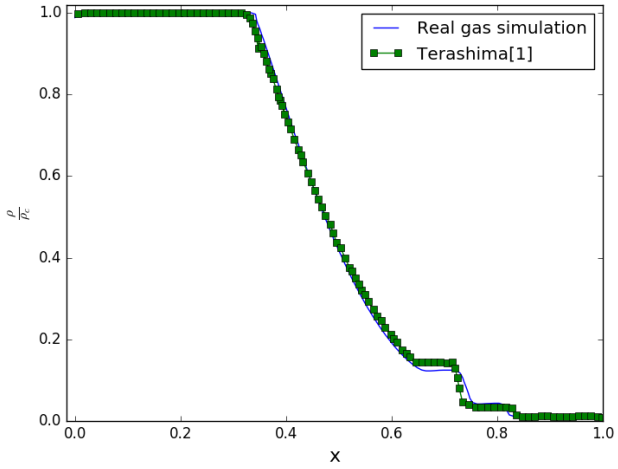

Figure 3. Normalized density vs distance plot for sod shocktube problem

There is a good agreement in between the present solver and the reference simulation data obtained from the paper, no spurious pressure oscillations are found mainly due to the fact that the initial conditions are in supercritical regime. However, the transcritical case showed significant pressure oscillations.

Another case used for reference is Shu-Osher problem[1] that is modified to the supercritical regime (initial conditions). The purpose of testing with this case is to validate the solver's dissipation characteristics. This test case is taken from Terashima[1], Nitrogen is used as working fluid for this case and the initial conditions are,

$$(\rho, u, p) = \begin{cases} (3.857\rho_0, M_{ref}, 10.333p_0) & -0.5 \leq x \leq -0.4 \text{ m}, \\ ((1.0 + 0.2sin5x)\rho_0, 0.0, p_0) & -0.4 \leq x \leq 0.5 \text{ m} \end{cases}$$

Here, $\rho_0 = 50.0\frac{Kg}{m^3}$, $p_0 = 4.0MPa$ and M_{ref} is the reference sound speed on the left side. Similarly as previous case, the grid consists of 2001 x 4 uniformly distributed cells. The below plot is taken at 5.903E-04 s.

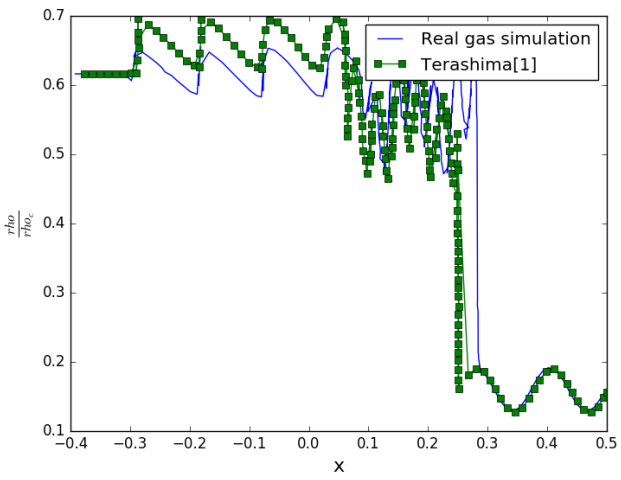

Figure 4. Normalized density vs distance plot for shu-osher shocktube problem

Figure 4 shows the normalized density ($\frac{\rho}{\rho_{crit}}$) plot for the current real fluid modified solver vs the reference case. It is important to mention here that the reference case was obtained by smoothening the initial interface with an adjustable free parameter $c_\epsilon = 3.0$. This could be a reason for slight mismatch in the density profiles.

2. Real fluid effects on the shock tube problem

Inorder to study the real fluid effects on shock tube wave propagation we simulated three cases, the supercritical, nearcritical and the subcritical thermodynamic conditions. The initial conditions are shown in the table 1 for each case, in all the cases the left to right pressure ratios are set to 2.

Table I. Initial conditions

	P_{left}	P_{right}	P_{left}/P_{right}	T,K	ρ_{left}	ρ_{right}
Supercritical	$4p_{cr}$	$2p_{cr}$	2	310	845	696
Nearcritical	$1.5p_{cr}$	$0.75p_{cr}$	2	310	610	134
Subcritical	$0.5p_{cr}$	$0.25p_{cr}$	2	310	76.9	34.4

Figures 5, 6 are the sod shock tube and Shu-Osher problem simulated for both ideal gas and real fluid equation of states for a supercritical thermodynamic condition. There's not much of difference for the sod shock tube case but there's a significance influence of real fluid equation of state in Shu-Osher problem primarily due to the dissipation characteristics.

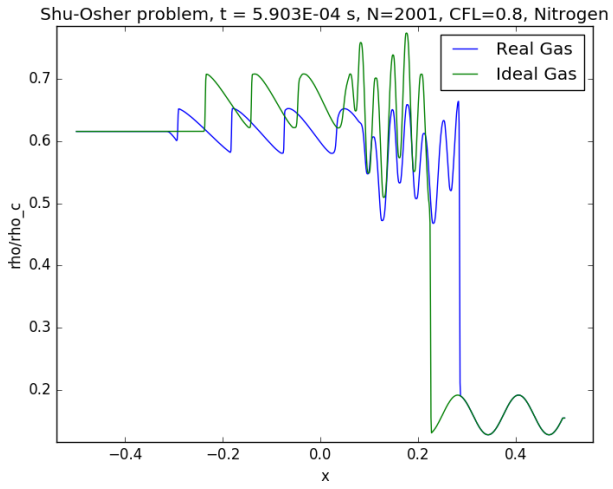

Figure 5. Normalized density vs distance plot for shu-osher shocktube problem

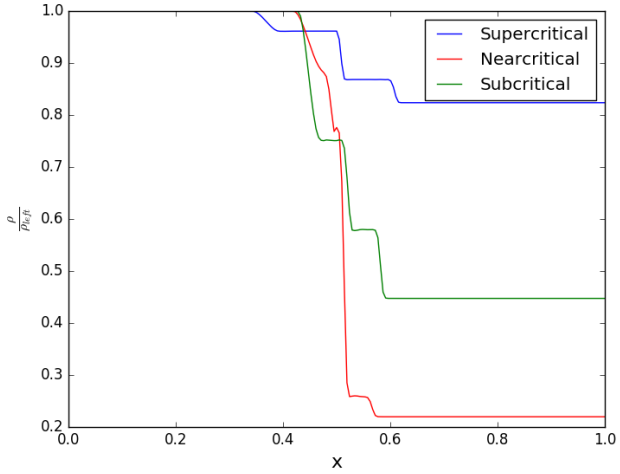

Figure 7. Normalized density vs distance plot for sod shocktube problem

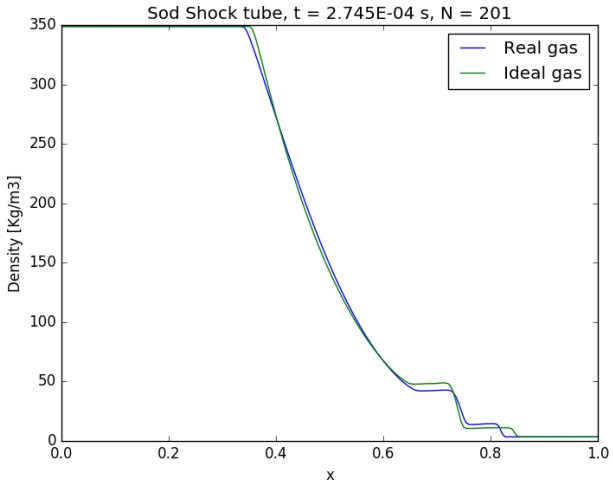

Figure 6. Normalized density vs distance plot for shu-osher shocktube problem

Figures 7,8,9 are the above mentioned three thermodynamic cases, supercritical, nearcritical, subcritical. The density, pressure, temperature are plotted for their non-dimensional values (with respect to the left side values) over the distance.

The density plots clearly show the three waves in all the three cases, however for the nearcritical case, the discontinuity is not yet fully resolved in the same time as others i.e., at t = 2.745E-04 s. Also, there is a large density jump at the contact discontinuity in comparison to the other cases and small density jump for the shock wave. However, the near critical case has small temperature change at the shock and contact discontinuity. For the supercritical case and the subcritical cases, the pressure jumps at the shock wave and contact discontinuity are quite similar but not when compared to the near critical case, which significantly has influence of the real fluid equation of state (strong non-linear variation of thermodynamic properties near the critical point) When the contact surface passes through the critical point, the density increases rapidly even with a small temperature decrease.

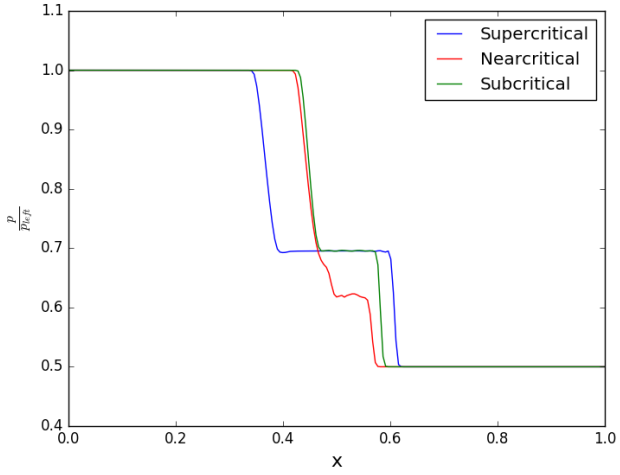

Figure 8. Normalized Pressure vs distance plot for sod shocktube problem

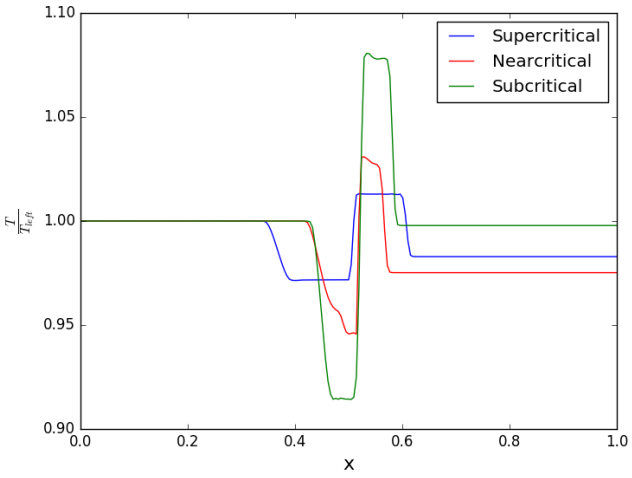

Figure 9. Normalized Temperature vs distance plot for sod shocktube problem

3. Shock wave propagation at the supercritical condition

Figure 10 plots the time histories of temperature profile in the supercritical case, the present solver successfully captured the temperature jumps,

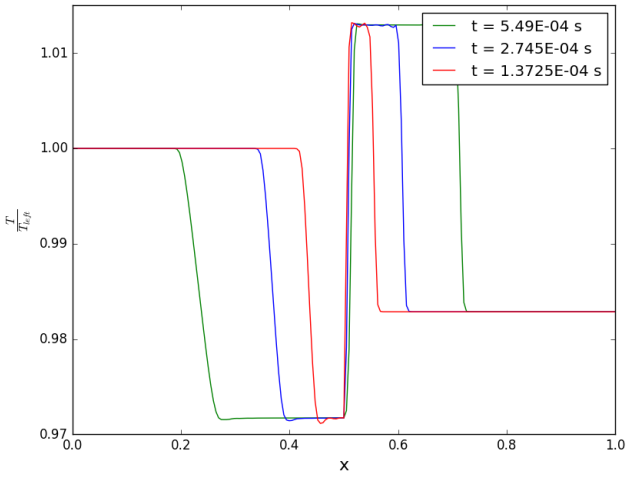

Figure 10. Time histories for temperature profile for supercritical case

Figure 11 plots the time histories of wave positions in comparison to three cases. It can be said that all the three waves (expansion fan, shock wave, contact discontinuity) are moving proportionally with respect to time. Among the three cases, the nearcritical case's expansion fan and the shock wave propagate much faster than the other cases. This could be explained by the variation of sound speed in the nearcritical case, due to the strong non-linear variation of density the speed of sound also varies non-linearly.

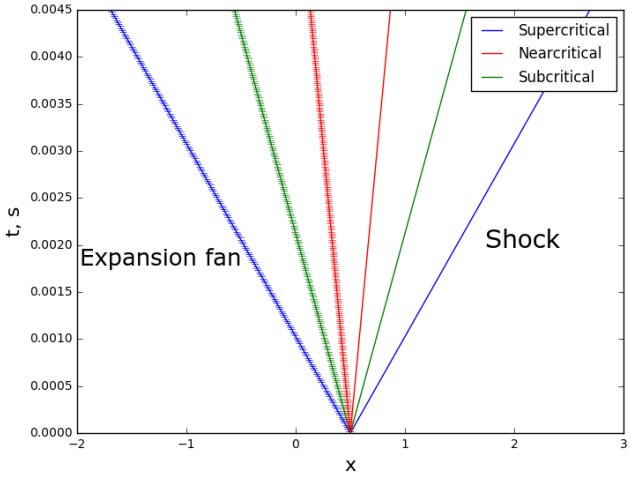

Figure 11. Time histories of shock and expansion fan positions

IV. CONCLUSION

A numerical solver for the supercritical fluid flow is developed with an extended HLLC riemann solver for real fluids with different equation of states. The solver is validated with two reference cases for the shock wave propagation, dissipation characteristics in the supercritical fluid condition. Using this solver, the shock tube problem is studied for three different thermodynamic cases, supercritical, nearcritical and subcritical. We observed that there is a large density change for a given small increment in temperature at the contact discontinuity where the fluid crosses the critical point. Primarily because of the non-linear variation of thermodynamic properties of nearcritical fluids. There is a significant effect of having real fluid thermodynamics especially when the initial conditions are near the critical point.

REFERENCES

[1]Terashima, H., Kawai, S., Yamanishi, N. (2011). High-resolution numerical method for supercritical flows with large density variations. AIAA journal, 49(12), 2658-2672.

[2]Gottlieb, S. and Shu, C.-W. Total variation diminishing Runge-Kutta schemes, Mathematics of Computation, 67 (1998), pp. 7386,.

[3]Toro E.F. (1997) The HLL and HLLC Riemann Solvers. In: Riemann Solvers and Numerical Methods for Fluid Dynamics. Springer, Berlin, Heidelberg

[4]Pure and Pseudo-pure Fluid Thermophysical Property Evaluation and the Open-Source Thermophysical Property Library CoolProp Ian H. Bell, Jorrit Wronski, Sylvain Quoilin, and Vincent Lemort Industrial Engineering Chemistry Research 2014 53 (6), 2498-2508 DOI: 10.1021/ie4033999

[5]Van Leer, B. (1977), "Towards the ultimate conservative difference scheme III. Upstream-centered finite-difference schemes for ideal compressible flow", J. Comp. Phys., 23 (3): 263275,

[6]P. Colella and H. M. Glaz. Efficient solution algorithms for the Riemann problem for real fluides. J Comput Phys, 59:264289, June 1985.

[7]Toro, E. F. (2013). Riemann solvers and numerical methods for fluid dynamics: a practical introduction. Springer Science Business Media.

[8]Lemmon, E., Huber, M., and McLinden, M., NIST Standard Reference Database 23: Reference Fluid Thermodynamic and Transport Properties-REFPROP, Version 8.0, National Institute of Standards and Technology, Standard Reference Data Program, Gaithersburg, MD, 2007

[9]Pantano, C., Saurel, R., Schmitt, T. (2017). An oscillation free shock-capturing method for compressible van der Waals supercritical fluid flows. Journal of Computational Physics, 335, 780-811.

[10]Arina, R. (2004). Numerical simulation of near-critical fluids. Applied numerical mathematics, 51(4), 409-426.

[11]Pizzarelli, Marco. (2010). Finite-volume solver of the euler equation for real fluids. International Journal of Applied Science Computations. 17. 68-91.

[12]Ma, P. C., Lv, Y., Ihme, M. (2017). An entropy-stable hybrid scheme for simulations of transcritical real-fluid flows. Journal of Computational Physics, 340, 330-357.

[13]Argrow, B. M. (1996). Computational analysis of dense gas shock tube flow. Shock Waves, 6(4), 241-248.

[14]Schlamp, S., Rsgen, T. (2005). Flow in near-critical fluids induced by shock and expansion waves. Shock Waves, 14(1-2), 93-101.

[15]Buffard, T., Gallout, T., Hrard, J. M. (2000). A sequel to a rough Godunov scheme: application to real fluides. Computers fluids, 29(7), 813-847.

[16]Terashima, H., Koshi, M. (2013). Strategy for simulating supercritical cryogenic jets using high-order schemes. Computers Fluids, 85, 39-46.

[17]Guardone, A., Vigevano, L., Argrow, B. M. (2004). Assessment of thermodynamic models for dense gas dynamics. Physics of Fluids, 16(11), 3878-3887.

[18]Almgren, A. S., Beckner, V. E., Bell, J. B., Day, M. S., Howell, L. H., Joggerst, C. C., ... Zingale, M. (2010). CASTRO: A new compressible astrophysical solver. I. Hydrodynamics and self-gravity. The Astrophysical Journal, 715(2), 1221.